

# Diffusion kurtosis imaging and diffusion-weighted imaging in assessment of liver fibrosis stage and necroinflammatory activity

Ruo Fan Sheng,<sup>1</sup> He Qing Wang,<sup>1</sup> Li Yang,<sup>1</sup> Kai Pu Jin,<sup>1</sup> Yan Hong Xie,<sup>2</sup>  
Cai Zhong Chen,<sup>1</sup> Meng Su Zeng<sup>1</sup>

<sup>1</sup>Department of Radiology, Zhongshan Hospital, Fudan University, Shanghai Institute of Medical Imaging, No. 180 Fenglin Road, Xuhui District, Shanghai 200032, China

<sup>2</sup>Department of Pathology, Zhongshan Hospital, Fudan University, No. 180 Fenglin Road, Xuhui District, Shanghai 200032, China

## Abstract

**Purpose:** To investigate and compare the diagnostic value of diffusion kurtosis imaging (DKI) with diffusion-weighted imaging (DWI) in assessing and quantifying hepatic fibrosis.

**Methods:** Thirty rats were divided into the control group ( $n = 6$ ) and the fibrosis experimental groups ( $n = 6$  per group) with  $\text{CCl}_4$  administration for 2, 4, 6, and 8 weeks. Liver fibrosis stage (S) and necroinflammatory activity grade (G) were histopathologically determined. DKI and DWI were performed; mean apparent diffusion (MD), mean kurtosis (MK), and apparent diffusion coefficient (ADC) values were calculated. DKI parameters were compared with ADC values according to G/S scores.

**Results:** Strong inverse correlations were found between the degree of fibrosis and both MD and ADC ( $r = -0.840$  and  $r = -0.760$ ), while only weak correlation existed in MK ( $r = 0.405$ ). ROC analyses demonstrated the AUC in MD, MK, and ADC of 0.862, 0.684, 0.817 for identifying mild and severe fibrosis, and 0.757, 0.675, 0.733 for non-cirrhosis and cirrhosis, respectively. The degree of fibrosis was significantly correlated with  $\alpha$ -smooth muscle actin ( $\alpha$ -SMA) ( $P < 0.0001$ );  $\alpha$ -SMA had strong inverse correlation with MD ( $r = -0.723$ ), moderate inverse correlation with ADC ( $r = -0.613$ ), and very weak correlation with MK ( $r = 0.175$ ). Additionally, MD was strongly correlated with the necroinflammatory activity ( $r = -0.758$ ), ADC was moderately correlated ( $r = -0.492$ ), and MK was weakly correlated ( $r = 0.254$ ).

**Conclusion:** DKI may provide added information and serve as a valuable tool for the characterization and surveillance of liver fibrosis in a non-invasive manner.

**Key words:** Liver—Fibrosis—Diffusion kurtosis imaging—Diffusion-weighted imaging

Liver fibrosis is a necessary stage to cirrhosis in response to repetitive liver injury from various causes [1], and the key factors in fibrogenesis are the activation and proliferation of hepatic stellate cells, which are characterized by  $\alpha$ -smooth muscle actin ( $\alpha$ -SMA) expression [2]. Cirrhosis substantially increases the risk of hepatocellular carcinoma (HCC), and the severity of liver fibrosis affects the prognosis of liver cancer surgery [3]. Nowadays, hepatic fibrosis is regarded as a dynamic process with potential for regression [1, 4]. Thus, early and accurate assessment of liver fibrosis, which can prevent and even reverse the proceeding, is of great clinical value.

Liver biopsy has been regarded as the reference standard for the diagnosis of liver fibrosis, but as an invasive means, biopsy can lead to potentially life-threatening complications. In addition, problems including sampling errors, inter-/intra-observer variability, and low patient acceptance limit its application [5]. Meanwhile, methods using usual laboratory data have been reported to predict significant fibrosis or cirrhosis. However, the serum biomarkers are not liver specific and are unable to discriminate between intermediate stages of fibrosis [6]. Nowadays, the emergence of new multiparameter MR imaging technologies makes the non-invasive evaluation of liver fibrosis a reality.

Diffusion-weighted imaging (DWI) has been regarded as a promising technique in the visualization of the cellular density and properties of the extracellular matrix, but one limitation of standard DWI is that apparent diffusion coefficient (ADC) is calculated using a monoexponential analysis, which assumes Gaussian behavior of water diffusion [7]. Diffusion kurtosis imaging (DKI) is an advanced DWI model that quantifies the non-Gaussian behavior of diffusion and provides both a diffusion coefficient as well as the excess kurtosis of tissue [8]. In this model,  $D$  represents corrected ADC accounting for non-Gaussian diffusion behavior and  $K$  represents excess kurtosis, reflecting the deviation from an ideal Gaussian curve [7]. It is believed that the DKI model may provide an opportunity to gain further insights into the states of liver diffusivities and tissue microstructural complexity than standard DWI [7]; but its application in liver is scarce with most limited to the *in vitro* studies [7, 9, 10].

Until now, there are still no acknowledged non-invasive approaches in fibrosis assessment, and rare study has been reported on the clinical application of DKI in it [10], especially *in vivo*. Therefore the purpose of this study was to investigate and compare the diagnostic value of DKI with conventional DWI in assessing and quantifying hepatic fibrosis, as well as the potential influence of necroinflammatory activity.

## Materials and methods

### *Animal model*

The institutional animal care and use committee of our institute approved this study. Thirty male 8-week-old Sprague-Dawley rats (ca. 250–280 g) were randomly divided into 4 experimental groups and 1 control group, consisting 6 rats per group. The rats in the experimental groups were administrated 50% CCl<sub>4</sub> and olive oil intraperitoneally twice a week at the dose of 1.5 ml/kg, for 2, 4, 6, and 8 weeks, respectively. Rats in the control group were administrated equal dose of olive oil for 8 weeks [11, 12].

### *Image acquisition*

MRI was performed using a 3.0-T scanner (Verio, Siemens, Erlangen, Germany) with a phased-array animal coil. DKI was performed with single-shot spin-echo echo-planar sequence using tridirectional motion-probing gradients with 6  $b$  values (0, 200, 500, 1000, 1500, and 2000 s/mm<sup>2</sup>) and the following parameters: TR/TE 5100/96.8 ms, slice thickness 2.0 mm, interslice gap 0.5 mm, field of view 138 × 138 mm, matrix 148 × 148. DWI was acquired with a transverse single-shot spin-echo echo-planar sequence (TR/TE = 5100/96.8 ms, slice thickness, 2.0 mm, interslice gap 0.5 mm, field of view 137 × 137 mm) with two  $b$  values (0 and 800 s/mm<sup>2</sup>).

### *Imaging analysis*

DICOM images from the DKI sequence were postprocessed using in-house software programmed in MeVisLab (Version 1.2.0; MeVis Medical Solutions AG, Bremen, Germany). This program performed voxel-by-voxel analysis, fitting diffusion-weighted signal intensities as a function of  $b$  value using the equation:  $S = S_0 \times \exp(-b \times D + b^2 \times D^2 \times K/6)$ , where  $b$  represents  $b$  value,  $D$  represents corrected ADC accounting for non-Gaussian diffusion behavior, and  $K$  represents excess kurtosis. Through this calculation, the program outputs maps for each explant of  $D$  and  $K$  and automatically outputs the values by measuring the region of interest (ROI). All images were analyzed by two abdominal radiologists (M.S.Z. and H.Q.W. with 31 and 16 years of experience in abdominal imaging) in a blinded manner. The readers were blinded to the group of the animal and pathology reports. The largest liver crosssection was chosen, and four ROIs measuring 0.1 cm<sup>2</sup> were drawn on the right lateral lobe, right median lobe, left median lobe, and left lateral lobe to measure the  $D$  and  $K$  coefficients as well as ADC of liver parenchyma, avoiding large vessels, lesions, artifacts, and the border of the liver. The average values—the mean apparent diffusion (MD), mean kurtosis (MK), and mean ADC values—were used.

### *Pathological analysis*

After MR examination, the rats were all humanely killed. The livers were removed and subsequently fixed in phosphate-buffered 10% formalin. Liver samples were stained with haematoxylin–eosin (HE) as well as Masson's trichrome stains. All pathologic specimens were reviewed by a pathologist (Y.H.X with 8 years of experience in liver pathology). The fibrosis stage (“S” grade) and the necroinflammatory activity (“G” grade) were evaluated by the METAVIR scoring system [13]. The degree of fibrosis was assessed using a scale ranging from 0 to 4 (0 = no fibrosis; 1 = mild fibrosis, portal fibrosis without septa; 2 = substantial fibrosis, periportal fibrosis and few septa; 3 = advanced fibrosis, septal fibrosis without cirrhosis; 4 = widespread fibrosis, cirrhosis). The degree of necroinflammatory activity was graded on a scale of 0 to 3 (0 = absent, 1 = mild activity, 2 = moderate activity, 3 = severe activity).

Immunostaining was performed for  $\alpha$ -SMA (1:1000; Abcam, UK). The degree and distribution of staining-positive cells (positive cytoplasm staining) were determined referring to the grading of fibrosis (0 = none, 1 = portal distribution, 2 = periportal and rare septal distribution, 3 = septal distribution, 4 = widespread distribution).

### Statistical analysis

All statistical analyses were performed using SPSS 22.0 (Chicago, IL, USA). Spearman's rank correlation test was used to measure the strength of the linear relationship between MR imaging parameters and the degree of fibrosis and necroinflammatory activity. Correlation coefficients were classified by absolute value as follows: 0.0–0.2, very weak to negligible correlation; 0.2–0.4, weak correlation; 0.4–0.7, moderate correlation; 0.7–0.9, strong correlation; 0.9–1.0, very strong correlation [14]. Kendall's Tau-b correlation coefficient was used to assess the relationship between the degree of fibrosis and  $\alpha$ -SMA staining. The MD, MK, and ADC values were compared between mild fibrosis ( $S \leq 2$ )/severe fibrosis ( $S \geq 3$ ), and non-cirrhosis (S1-3)/cirrhosis (S4) subgroups using the student's  $t$  test when normally distributed or Mann–Whitney U test when non-normally distributed. Additionally, receiver operating characteristic (ROC) analysis and corresponding area under the curve (AUC) statistics were applied to determine the discriminatory

accuracy of the MR imaging parameters above regarding diagnostic performance. Optimal cutoff values were chosen to maximize the sum of sensitivity and specificity. The difference in diagnostic performance was analyzed by comparing the ROC curves. Interobserver agreement for the quantitative parameters measured by two observers independently was assessed by the intraclass correlation coefficient (ICC). All tests were two-sided, and  $P < 0.05$  was considered statistically significant.

### Results

Histopathologically, 6, 6, 5, 6, 7 rats were diagnosed as S0–S4 (Fig. 1), and 13, 5, 6, 6 rats were diagnosed as G0–G3, respectively. Steatosis content more than 5% was found in only 2 cases.

#### MR parameters and fibrosis

Image quality of hepatic DKI was satisfied (Fig. 2). Strong inverse correlations were found between the de-

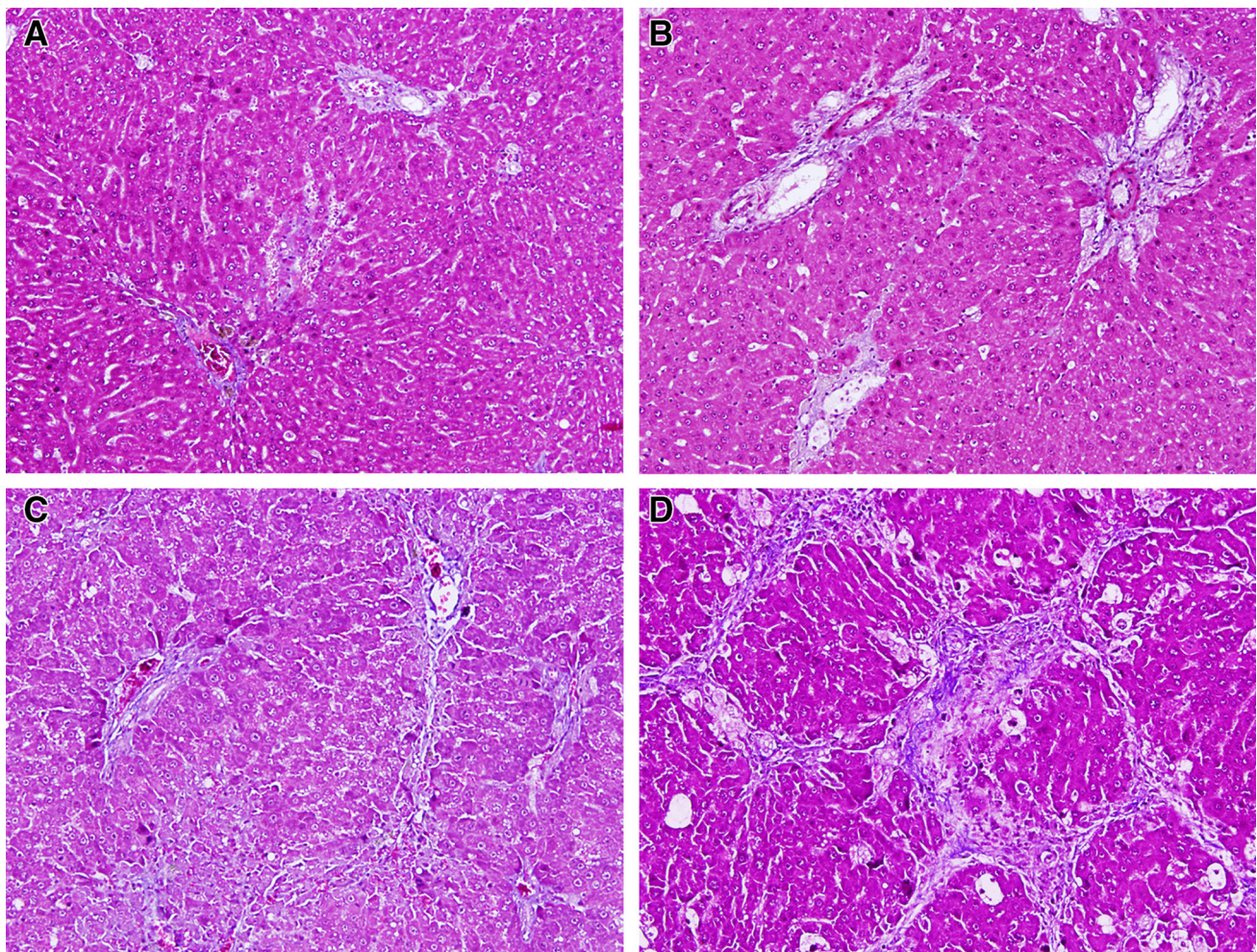


**Fig. 1.** Masson's trichrome staining ( $\times 100$ ) grading **A** S1, portal fibrosis; **B** S2, periportal fibrosis and few septa; **C** S3, septal fibrosis bridging portal triads and central veins; and **D** S4, cirrhosis.

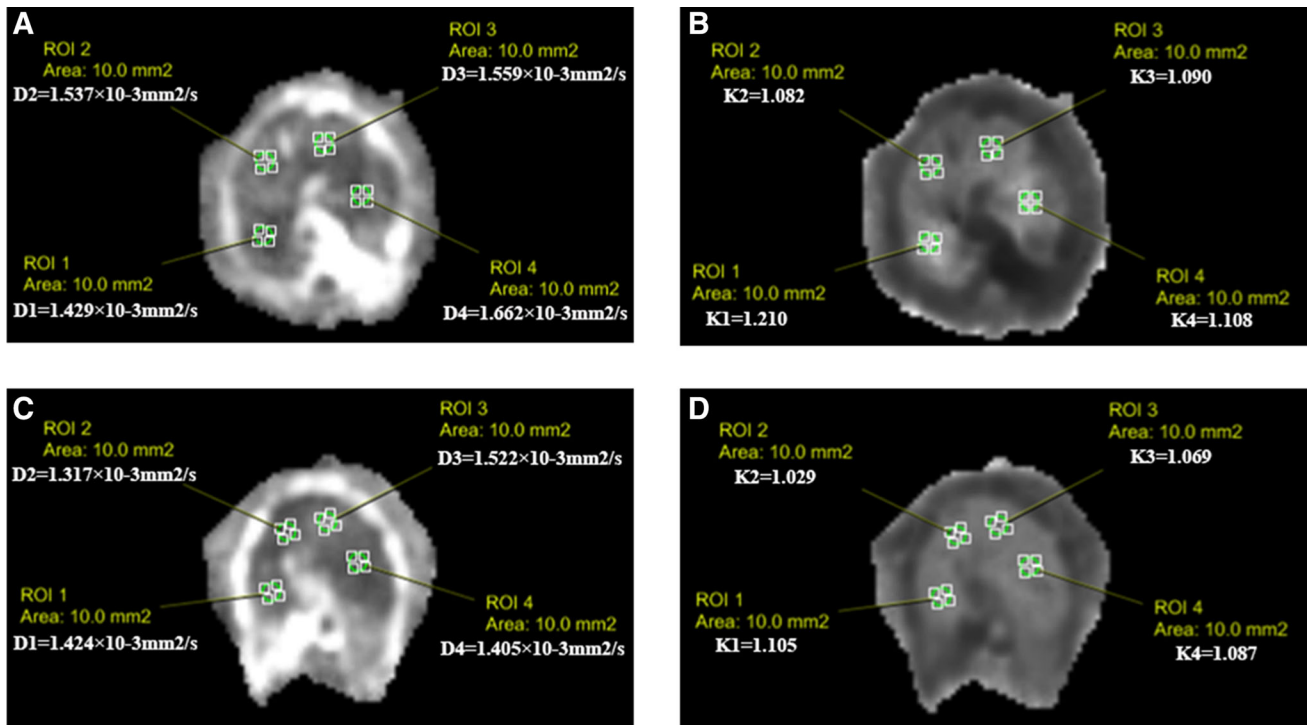


Fig. 2. Examples of placement of regions of interest (ROIs) and the corresponding results on diffusion kurtosis imaging parametric maps of **A, C** the apparent diffusion coefficient (D

map) and **B, D** kurtosis coefficient (K map) in two rats grading G0S1 (**A, B**) and G3S4 (**C, D**).

Table 1. Mean values and standard deviation (SD) of MD, MK, and ADC values of the liver parenchyma

	Mild fibrosis ( $S \leq 2$ )	Severe fibrosis ( $S \geq 3$ )	Non-cirrhosis (S1-3)	Cirrhosis (S4)
MD ( $\times 10^{-3} \text{ mm}^2/\text{s}$ )	1.614	1.416	1.497	1.385
SD	0.151	0.129	0.106	0.128
MK	1.084	1.133	1.129	1.106
SD	0.066	0.058	0.055	0.034
ADC ( $\times 10^{-3} \text{ mm}^2/\text{s}$ )	1.110	0.999	1.039	0.975
SD	0.099	0.074	0.074	0.063

MD mean apparent diffusion, MK mean kurtosis, ADC, apparent diffusion coefficient

gree of fibrosis and both MD and ADC ( $r = -0.840$ ,  $P < 0.0001$  and  $r = -0.760$ ,  $P < 0.0001$ ), while only weak correlation existed in MK ( $r = 0.405$ ,  $P = 0.032$ ).

*Diagnostic performance for assessment of mild ( $S \leq 2$ ) and severe fibrosis ( $S \geq 3$ )*

Mean values of MD and ADC showed significant differences between mild and severe S scores ( $t = 3.428$ ,  $P = 0.0022$  and  $t = 3.352$ ,  $P = 0.0024$ ), while the MK value was not significantly different ( $t = 1.999$ ,  $P = 0.0562$ ) (Table 1). ROC analyses demonstrated AUCs of 0.862 (95% CI 0.722–1.000;  $P = 0.002$ ), 0.684 (95% CI 0.479–0.890;  $P = 0.105$ ), and 0.817 (95% CI 0.657–0.977;  $P = 0.004$ ) in MD, MK, and ADC values for the identification of mild and severe S scores, respectively (Fig. 3A). Excellent discrimination existed in

MD and ADC. When the optimal cutoff values of  $1.538 \times 10^{-3} \text{ mm}^2/\text{s}$  (MD) and  $1.030 \times 10^{-3} \text{ mm}^2/\text{s}$  (ADC) were used, the sensitivity of 75.0% and 87.5% and specificity of 90.0% and 76.9% can be achieved. But no differences were found in the comparison of ROC curves using MD and ADC ( $F = 0.058$ ,  $P = 0.810$ ).

*Diagnostic performance for assessment of non-cirrhosis (S1-3) and cirrhosis (S4)*

Mean values of MD, MK, and ADC showed no significant differences between non-cirrhosis and cirrhosis groups ( $U = 17$ ,  $P = 0.1052$ ;  $t = 0.8725$ ;  $P = 0.3938$ ; and  $t = 1.987$ ,  $P = 0.0608$ , respectively) (Table 1), while ROC analyses demonstrated AUCs of 0.757 (95% CI 0.522–0.992;  $P = 0.096$ ), 0.675 (95% CI 0.438–0.912;  $P = 0.248$ ), and 0.733 (95% CI 0.513–0.954;  $P = 0.084$ )

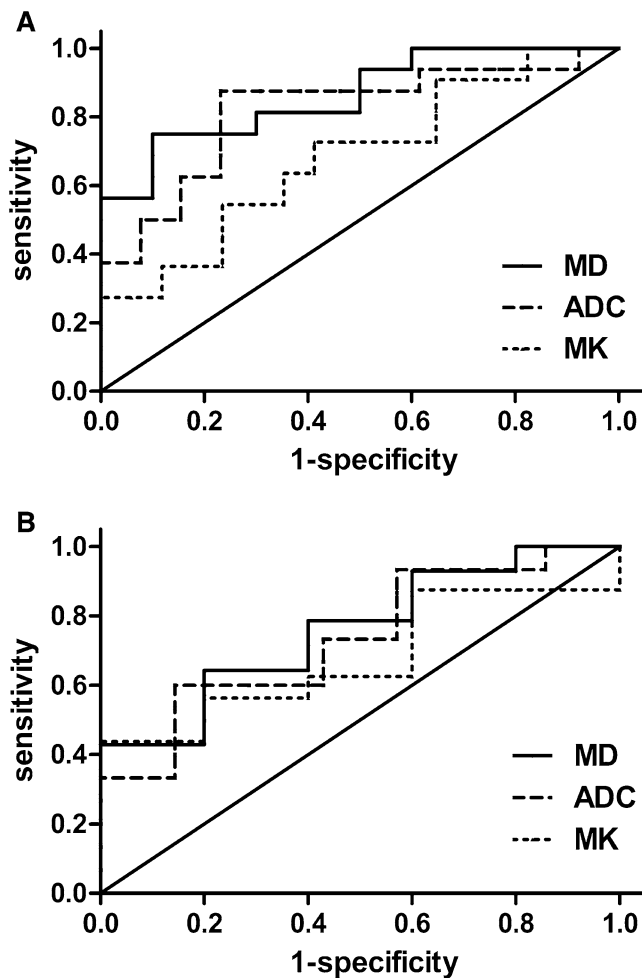


Fig. 3. ROC and AUC values for the identification of **A** mild fibrosis ( $S \leq 2$ ) and severe fibrosis ( $S \geq 3$ ), and **B** non-cirrhosis (S1-3) and cirrhosis (S4) using MD, ADC, and MK. MD mean apparent diffusion, ADC apparent diffusion coefficient, MK mean kurtosis.

in MD, MK, and ADC values for identification of non-cirrhosis and cirrhosis, respectively (Fig. 3B). MD and ADC had acceptable discrimination in identifying non-cirrhosis and cirrhosis. When the optimal cutoff values of  $1.498 \times 10^{-3} \text{ mm}^2/\text{s}$  (MD) and  $1.030 \times 10^{-3} \text{ mm}^2/\text{s}$  (ADC) were used, the sensitivity of 64.3% and 60.0% and specificity of 80.0% and 85.7% can be achieved. No significant differences were found in the comparison of ROC analyses of the three curves ( $F = 1.363$ ,  $P = 0.264$ ).

#### Correlation analyses regarding $\alpha$ -SMA

The degree of fibrosis was significantly correlated with  $\alpha$ -SMA ( $P < 0.0001$ ) (Fig. 4). The expression of  $\alpha$ -SMA had strong inverse correlation with MD ( $r = -0.723$ ,  $P < 0.0001$ ), moderate inverse correlation with ADC ( $r = -0.613$ ,  $P < 0.0001$ ), but no linear correlation with MK ( $r = 0.175$ ,  $P = 0.374$ ).

#### MR parameters and necroinflammatory activity

Meanwhile, MD was strongly correlated with necroinflammatory activity ( $r = -0.758$ ,  $P < 0.0001$ ), ADC was moderately correlated ( $r = -0.492$ ,  $P = 0.007$ ), and MK was not linearly correlated ( $r = 0.254$ ,  $P = 0.192$ ).

Satisfactory interobserver agreement between observers was obtained for MD and ADC with ICC of 0.800 and 0.881, while weaker agreement was found in MK with ICC of 0.616.

## Discussion

The key element of liver fibrosis in an efficient treatment is a reliable diagnostic method that allows accurate staging to follow disease progression or response to therapy. As fibrosis is recognized as a dynamic process with a high potential for partial or complete resolution before developing into cirrhosis [15], and the risk of various complications would increase dramatically if patients reached the stage of cirrhosis, we first made a comparison between non-cirrhotic fibrosis and cirrhosis. Additionally, the diagnosis of S3 or greater fibrosis is clinically important for the adoption of antiviral therapy and the monitoring of liver function after antiviral therapy [3, 16]; a comparison between mild fibrosis ( $S \leq 2$ ) and severe fibrosis ( $S \geq 3$ ) was also done in our study.

Standard DWI enables the visualization of diffusivity of water molecules, providing information regarding the cellular microstructure and properties of the extracellular matrix. The diffusion characteristics may provide both functional and microstructural information [17]. But the model is calculated using a monoexponential analysis, which assumes Gaussian behavior of water diffusion. However, a deviation from a simple monoexponential decay is readily identified in the liver, DKI provides a new model in assessing non-Gaussian diffusion behavior. Rosenkrantz et al. [7] and Goshima et al. [9] assessed HCC ex vivo and in vivo, respectively, and considered DKI an effective technique to identify the heterogeneity of cellularity and microstructural complexity. Anderson et al. [10] examined animal models of hepatic fibrosis and found DKI a superior model fit when compared to either the stretched exponential or monoexponential models, but their research was undertaken ex vivo. Until now, no data were provided regarding the application of DKI in liver fibrosis in vivo.

The results of the present study revealed that MD and ADC significantly correlated with fibrosis degrees and the expression of  $\alpha$ -SMA, and had good discrimination in the differentiation of mild/severe fibrosis and non-cirrhosis/cirrhosis. It can be explained by the restricted water diffusion in the presence of increased extracellular collagen deposition, narrowed sinusoids, and decreased

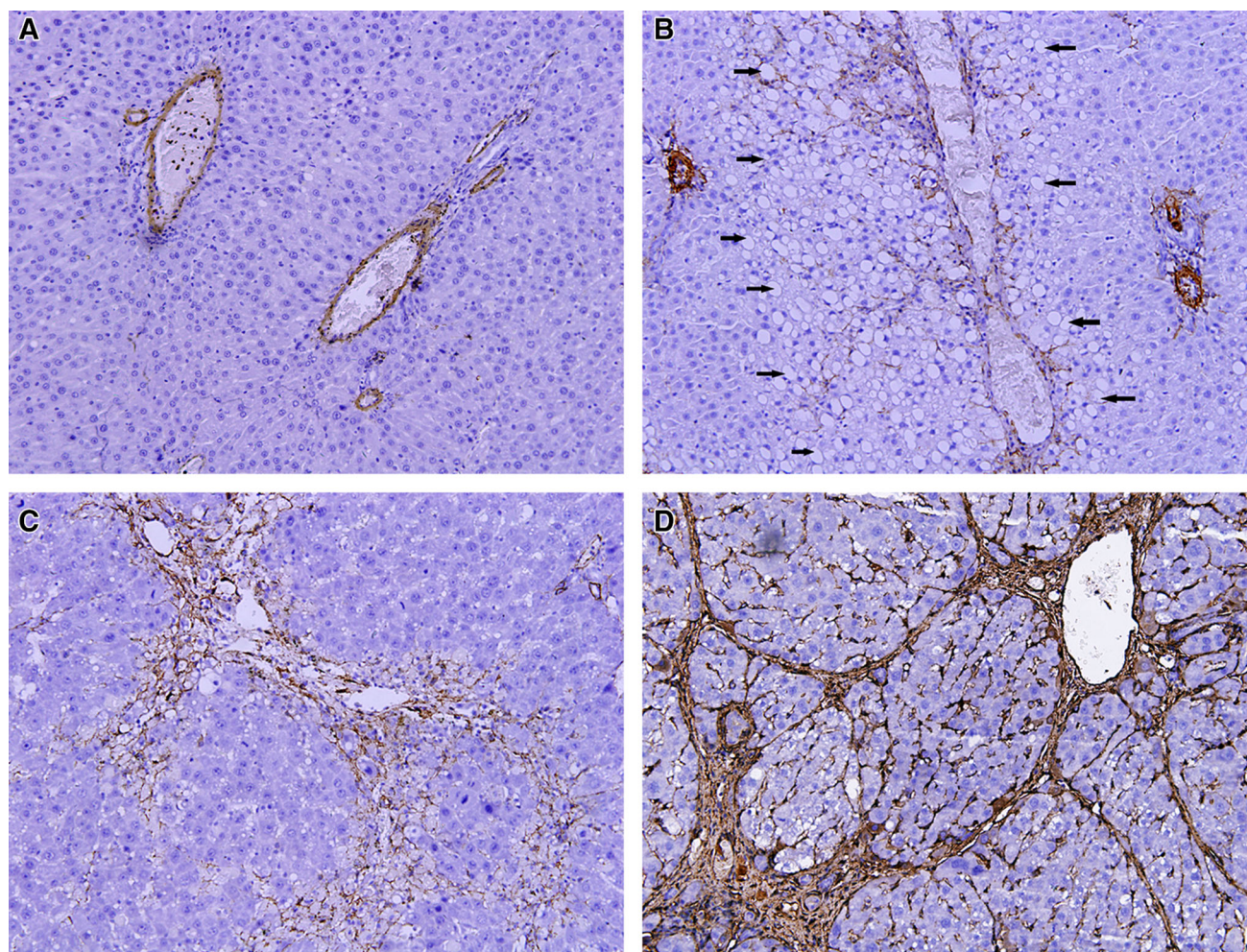


**Fig. 4.** Immunohistochemical staining ( $\times 100$ ) of  $\alpha$ -SMA with **A** grade 1, portal distribution; **B** grade 2, periportal and rare septal distribution; **C** grade 3, septal distribution; and **D** grade

**4,** widespread distribution. Notice the accompanying steatosis in one case (**B**, *black arrows*).

blood flow in the state of fibrosis[18]. In addition, MD showed better performance than ADC with relatively larger AUC and stronger correlations, which coincided with Anderson et al. [10], although no significant differences were found. Our results also showed higher specificity of MD than ADC in distinguishing mild and severe fibrosis and the possible explanations may be that ADC correlates are not specific for the effects of cellularity on water motion, which can also be hindered simply by the presence of a greater concentration of macromolecules and increased viscosity; while MD not only potentially better reflects water diffusivity in tissues at ultrahigh  $b$  values, but also contains specific information on the non-Gaussian diffusion behavior [19]. Thus, MD in DKI may give added information from that provided by ADC. We hypothesized that it could be used to determine the indication of anti-fibrosis treatment and as a marker for therapy surveillance.

MK represents excess kurtosis, but it only had weak correlation with and poor discrimination capacity in

fibrosis. This may partly be explained by the overlap in structural heterogeneity among varying degrees of fibrosis, the technical instability given the respiratory motion artifact and insufficient signal-to-noise ratio at high  $b$  values [7], as well as higher uncertainty of this parameter as poorer reproducibility was found in MK of our study. This result was contrary to that of Anderson et al. [10], but their research was carried out on liver specimens *ex vivo*, thereby inducing alterations to the observed hepatic kurtosis coefficients. Further studies are needed to confirm our viewpoint.

Another finding was that the MR parameters were more strongly correlated with fibrosis degrees than with necroinflammatory activity. The reasons may be as follows: necroinflammation is a continuous process, it could be evaluated by portal tract inflammation, interface hepatitis, and lobular inflammation. It may be a past event that has stabilized or even regressed or is an ongoing process that may worsen. Therefore, it is difficult to divide the stage clearly [3, 20]. In addition, the

influence of complex cellular topology and polydispersity may also influence the results.

This study had several limitations. First, the sample size was relatively small, thus detailed analysis between different fibrosis stages was not achieved. Second, although data from animal models are valuable, it has to be taken into account that the kinetics of regeneration differs between humans and rodents. Additionally, fibrosis and cirrhosis in humans often take place in chronic liver disease including hepatitis B or C. Further study of this technique in humans, especially with chronic liver disease is warranted to fully explore its potential clinical utility. Third, non-parenchymal cells as well as other phenomena occurring in the interstitial space such as steatosis were not evaluated in the present study. But only two in our cases had steatosis content more than 5%, and Lee et al. [21] indicated that hepatic steatosis did not affect measurement of diffusion and was unlikely to confound the diagnosis of hepatic fibrosis.

In conclusion, DKI may provide added information and serve as a valuable tool for the characterization and surveillance of liver fibrosis in a non-invasive manner.

#### Compliance with ethical standards

**Funding** This study was funded by the National Natural Science Foundation for Young Scientists of China (grant number 81601488), the Shanghai Sailing Program (grant number 16YF1410600), and the National Natural Science Foundation of China (grant number 81571661).

**Conflict of interest** The authors declare that they have no conflict of interest.

**Ethical approval** All applicable international, national, and/or institutional guidelines for the care and use of animals were followed. All procedures performed in studies involving animals were in accordance with the ethical standards of the institution or practice at which the studies were conducted.

**Informed consent** Statement of informed consent was not applicable since the manuscript does not contain any patient data.

#### References

- Faria SC, Ganesan K, Mwangi I, et al. (2009) MR imaging of liver fibrosis: current state of the art. *Radiographics* 29:1615–1636
- Li F, Song Z, Li Q, et al. (2011) Molecular imaging of hepatic stellate cell activity by visualization of hepatic integrin  $\alpha_v\beta_3$  expression with SPECT in rat. *Hepatology* 54:1020–1030
- Ding Y, Rao SX, Zhu T, et al. (2015) Liver fibrosis staging using T1 mapping on gadoxetic acid-enhanced MRI compared with DW imaging. *Clin Radiol* 70:1096–1103
- Trautwein C, Friedman SL, Schuppan D, Pinzani M (2015) Hepatic fibrosis: concept to treatment. *J Hepatol* 62:S15–S24
- Yoon JH, Lee JM, Baek JH, et al. (2014) Evaluation of hepatic fibrosis using intravoxel incoherent motion in diffusion-weighted liver MRI. *J Comput Assist Tomogr* 38:110–116
- Venkatesh SK, Wang G, Lim SG, Wee A (2014) Magnetic resonance elastography for the detection and staging of liver fibrosis in chronic hepatitis B. *Eur Radiol* 24:70–78
- Rosenkrantz AB, Sigmund EE, Winnick A, et al. (2012) Assessment of hepatocellular carcinoma using apparent diffusion coefficient and diffusion kurtosis indices: preliminary experience in fresh liver explants. *Magn Reson Imaging* 30:1534–1540
- Jensen JH, Helpert JA, Ramani A, Lu HZ, Kaczynski K (2005) Diffusional kurtosis imaging: the quantification of non-Gaussian water diffusion by means of magnetic resonance imaging. *Magn Reson Med* 53:1432–1440
- Goshima S, Kanematsu M, Noda Y, et al. (2015) Diffusion kurtosis imaging to assess response to treatment in hypervascular hepatocellular carcinoma. *AJR Am J Roentgenol* 204:W543–W549
- Anderson SW, Barry B, Soto J, et al. (2014) Characterizing non-Gaussian, high b-value diffusion in liver fibrosis: stretched exponential and diffusional kurtosis modeling. *J Magn Reson Imaging* 39:827–834
- Lagadec M, Doblas S, Giraudeau C, et al. (2015) Advanced fibrosis: correlation between pharmacokinetic parameters at dynamic gadoxetic acid-enhanced MR imaging and hepatocyte organic anion transporter expression in rat liver. *Radiology* 274:379–386
- Dong D, Yin L, Qi Y, Xu L, Peng J (2015) Protective effect of the total saponins from *Rosa laevigata* Michx fruit against carbon tetrachloride-induced liver fibrosis in rats. *Nutrients* 7:4829–4850
- Bedossa P, Poynard T (1996) An algorithm for the grading of activity in chronic hepatitis C. *Hepatology* 24:289–293
- Karlik SJ (2003) Exploring and summarizing radiologic data. *AJR Am J Roentgenol* 180:47–54
- Polasek M, Fuchs BC, Uppal R, et al. (2012) Molecular MR imaging of liver fibrosis: a feasibility study using rat and mouse models. *J Hepatol* 57:549–555
- Nishie A, Asayama Y, Ishigami K, et al. (2012) MR prediction of liver fibrosis using a liver-specific contrast agent: superparamagnetic iron oxide versus Gd-EOB-DTPA. *J Magn Reson Imaging* 36:664–671
- Cheung JS, Fan SJ, Chow AM, Hui ES, Wu EX (2009) In vivo DTI assessment of hepatic ischemia reperfusion injury in an experimental rat model. *J Magn Reson Imaging* 30:890–895
- Taouli B, Chouli M, Martin AJ, et al. (2008) Chronic hepatitis: role of diffusion-weighted imaging and diffusion-tensor imaging for the diagnosis of liver fibrosis and inflammation. *J Magn Reson Imaging* 28:89–95
- Rosenkrantz AB, Padhani AR, Chenevert TL, et al. (2015) Body diffusion kurtosis imaging: basic principles, applications, and considerations for clinical practice. *J Magn Reson Imaging* 42:1190–1202
- Guido M, Mangia A, Faa G (2011) Chronic viral hepatitis: the histology report. *Dig Liver Dis* 43(Suppl 4):S331–S343
- Lee JT, Liao J, Murphy P, et al. (2012) Cross-sectional investigation of correlation between hepatic steatosis and IVIM perfusion on MR imaging. *Magn Reson Imaging* 30:572–578